Consensus Vibration Control for Large Flexible Structures of Spacecraft With Modified Positive Position Feedback Control

Naiming Qi, Qiufan Yuan, Yanfang Liu, Mingying Huo, and Shilei Cao

***Abstract*— In this brief, consensus modified positive position feedback (CMPPF) is proposed to depress the vibration of large flexible structure in the spacecraft. CMPPF is formulated by decentralizing and distributing the modified positive position feedback (MPPF) to a network of control agents. Variables are appropriately selected and the consensus algorithm is employed to make the multiagents consensus with each other. CMPPF convergence conditions are derived and the control parameters are optimized. Amplitude-frequency response analysis and simulations demonstrate that CMPPF suppresses vibrations faster and more evidently than MPPF. Results also indicate how consensus between agents is realized and how agents' disagreement is eliminated. Effects of different consensus variables and different communication topologies are studied. Meanwhile, results for different types of agents' failure are presented. CMPPF is robust to topology and agents' failure and achieves satisfactory performances.**

***Index Terms*— Active vibration control (AVC), consensus control, flexible spacecraft, large flexible structures, modified positive position feedback (MPPF).**

I. Introduction

With rapid development of space technology, the structures in spacecraft are becoming larger and more flexible. New kinds of spacecrafts, such as space solar power plants and satellites with large flexible antennas, have extremely low vibration frequencies [1]. During the orbit keeping and attitude maneuvering, the disturbances from thrusters continuously excite the vibrations of the flexible structures [2]. In fast tracking and high-precision pointing tasks, the continuous force vibrations of flexible structures worsen the precision of attitude control and need to be suppressed.

Active vibration control (AVC) is an efficient way to suppress the vibration. In centralized AVC, there is only one controller referred as the central controller, which collects all the measured signals and computes all the control signals. Many efficient centralized control methods have been proposed, such as velocity feedback, resonant control, positive position feedback (PPF), and modified PPF (MPPF) [3], [4]. PPF is efficient for free vibration, but not for force vibration. Single-mode MPPF, proposed by Mahmoodi [4], reduces the force vibration to less than 23%. Some new control methods are proposed based on MPPF, such as adaptive MPPF and H_∞ MPPF [5], [6]. Besides, the advanced optimal methods, such as the linear quadratic regulator control and the pole placement method [7]–[10], are combined with AVC.

Although many efficient centralized active vibration controllers have been proposed, they have two limits for the large flexible structure. First, the sufficient computational power is required to handle the large number of actuators and sensors. Second, the disagreements of different actuator/sensor pairs worsen the control performance.

To deal with these two problems, the consensus algorithm is applied to AVC [11]–[13]. The consensus algorithm has been applied to many fields, such as the formation of unmanned aerial vehicles, robots, and satellites [14]–[17]. Among these fields, a large number of control agents collaborate with each other through two-stage control scheme [18]. An individual control algorithm is working at each agent stage. The consensus algorithm is realized in the network topology as the consensus stage. With this consensus algorithm, the calculating pressure is decentralized and different agents reach consensus. For multiagent AVC systems, the consensus PPF (CPPF) employs the consensus algorithm to enhance the individual PPF in each agent [11]. It consists of second-order filters and is more efficient and robust than the PPF controller. Compared with CPPF, the integral consensus controller (ICC) is simpler [12]. It employs the parallel first-order integrator filters and achieves the similar vibration suppression effect. Unlike that, the leader–follower consensus method utilizes a virtual leader and all agents follow it to enforce the vibration amplitude to zero [13]. It provides a better suppression effect than CPPF.

To supplement the existing research, the CMPPF controller is proposed in this brief as a combination of a very low-damping CPPF and an ICC. It consists of parallel second-order filters and parallel first-order integrator filters. In other words, CMPPF employs the consensus algorithm to enhance the MPPF controller. The individual controller is MPPF, decentralized to distribute on a network of control agents.

The development of CMPPF is to meet the needs of efficient vibration suppression for large flexible structures in the spacecraft. CMPPF constructs a multiagent control

Manuscript received September 28, 2017; revised February 21, 2018; accepted April 12, 2018. Date of publication May 8, 2018; date of current version June 11, 2019. This work was supported in part by the National Natural Science Foundation of China under Grant 11672093 and Grant 51705109, in part by the Special Foundation of Heilongjiang Postdoctoral Science under Grant LBH-TZ1609, in part by an innovation fund from the Shanghai Academy of Spaceflight Technology under Grant SAST 2015084, in part by the Fundamental Research Funds for the Central Universities under Grant HIT.NSRIF.201622, in part by the Open Fund of the National Defense Key Discipline Laboratory of Micro-Spacecraft Technology under Grant HIT.KLOF.MST.201507, and in part by the Seed Fund from the Qian Xuesen Laboratory of Space Technology. Recommended by Associate Editor Y. Ebihara. *(Corresponding authors: Qiufan Yuan; Yanfang Liu.)*

N. Qi, Y. Liu, M. Huo, and S. Cao are with the School of Astronautics, Harbin Institute of Technology, Harbin 150001, China (e-mail: qinmok@163.com; liu-yanfang@hotmail.com; huomingying@hit.edu.cn; caosl_hit@163.com).

Q. Yuan is with the School of Astronautics, Harbin Institute of Technology, Harbin 150001, China, and also with the Shanghai Aerospace System Engineering Institute, Shanghai 201109, China (e-mail: yuanqiufan@hotmail.com).

Color versions of one or more of the figures in this paper are available online at http://ieeexplore.ieee.org.

Digital Object Identifier 10.1109/TCST.2018.2830301

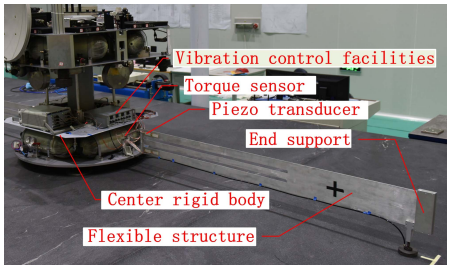

Fig. 1. Air-bearing experimental system for large-flexible spacecraft.

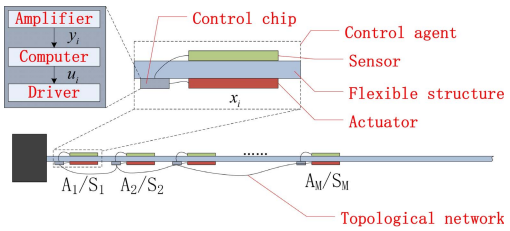

Fig. 2. Cantilever beam with control agents.

system, which is applicable for vibration control with the large numbers of actuators/sensors. This characteristic meets the needs of vibration control of large flexible structures. As the individual controller is MPPF, CMPPF is also very efficient to suppress the force vibration. Vibration amplitudes of the flexible structures can be largely reduced by CMPPF. Thus, the attitude control precision and stability are improved. As an extension of application, CMPPF can also be applied for synchronous vibration suppression of complex flexible structures, such as multisegment large flexible structures.

The remainder of the brief is organized as follows. In Section II, large flexible structure dynamics is modeled under the multiagent condition. In Section III, multiagent multimode MPPF controller is described. Then, the CMPPF controller is proposed. Convergence condition and parameters optimization are discussed. In Section IV, amplitude-frequency response (AFR) and simulations are carried out to verify the effectiveness of CMPPF.

II. MultiAgent Modeling of Large Flexible Structures

As shown in Fig. 1, the experimental system is used to study the vibration control of the large flexible spacecraft. The cantilever beam is the simplified structure of large flexible structures, such as solar panels and antennas. The composition of vibration control system is shown in Fig. 2. Piezoelectric layers are bonded to the beam in a collocated manner and perform as actuators and sensors. The system consists of several agents through a topological network. Each agent consists of an actuator, a sensor, and a controller chip. Each controller chip contains a charge amplifier, a computer, and a piezoelectric driver. The charge amplifier's output voltage is proportional to the stress in the sensor. The piezoelectric driver enlarges the control voltage to the driving voltage for the actuator.

The communication topology network is determined by the physical connections between agents. The adjacency matrix

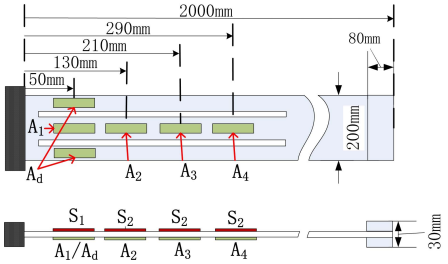

Fig. 3. Model structure for simulation.

TABLE I
Material and Structural Properties

	Parameter	Value
Plate	Density	2770 kg/m^3
	Thickness	0.002 m
	Young's modulus	70 GPa
	Damping ratio	0.003
Piezo patches	Material	PZT-5X
	Thickness	0.0002 m
	Length	60 mm
	Width	20 mm
	Young's modulus	61 GPa
	Piezoelectric coefficient	−320 PC/N

of the topology is introduced as $\bar{\boldsymbol{A}}_d = \{a_{ij}\} \in \mathbb{R}^{M\times M}$ with $a_{ij} = 1$ if there is a communication edge from agent j to agent i, namely, agent j is the parent of agent i, otherwise $a_{ij} = 0$ and $a_{ii} = 0$ with $i \in 1, \ldots, M$. The in-degree matrix is $\boldsymbol{D}_{\text{in}} = \text{diag}\{D_i\}$ and $D_i = \sum(\bar{A}_{di})$, $\bar{A}_{di}$ is the ith row of $\bar{\boldsymbol{A}}_d$. And the Laplacian matrix is defined by $\boldsymbol{L} = \boldsymbol{D}_{\text{in}} - \bar{\boldsymbol{A}}_d$. $\boldsymbol{L}$ describes the information exchange between different agents.

A simulation model is described here to provide a clear picture of the application. It is the same as the flexible structure in the experimental system, as shown in Fig. 3. Materials and structural properties are listed in Table I. Four agents are bonded on the surface of the beam. Actuators and sensors are defined as A_1 to A_4 and S_1 to S_4, respectively. Another two actuators A_d are bonded at the root of the beam to add disturbance. The corresponding finite-element model is built by the finite-element method (FEM) software Abaqus, with C3D10 element type, 7998 elements, and 15906 nodes. After imported to Adams, the FEM model is used to verify the controller based on Adams/Simulink co-simulation technique.

Considering the M actuator/sensor pairs and the first N modes, the state-space form of the vibration control system is

$$\begin{cases} \ddot{\boldsymbol{q}}(t) + \boldsymbol{H}\dot{\boldsymbol{q}}(t) + \boldsymbol{\Omega}^2\boldsymbol{q}(t) = \boldsymbol{\Psi}^T\boldsymbol{u}(t) + \boldsymbol{\psi}_d d(t) \\ \boldsymbol{y}(t) = \boldsymbol{\Psi}\boldsymbol{q}(t) \end{cases} \tag{1}$$

where $\boldsymbol{q}(t)$ is the vector of modal coordinates, $\boldsymbol{y}(t) \in \mathbb{R}^M$ is the vector of the amplifier's output voltages, and $\boldsymbol{u}(t) \in \mathbb{R}^M$ is the vector of the control signals. $\boldsymbol{H} = \text{diag}(\eta_k)$, $\eta_k = 2\zeta_k\omega_k$ with ζ_k and ω_k the damping ratio and modal frequency, respectively. $\boldsymbol{\Omega} = \text{diag}(\omega_k)$. $k \in \{1, 2, \ldots, N\}$. $d(t)$ and $\boldsymbol{\psi}_d$ are the disturbance and the vector of disturbance gains, respectively. $\boldsymbol{\Psi} \in \mathbb{R}^{M\times N}$ with the element at row i and column k is ψ_{ik}, $\psi_{ik} = \kappa(\varphi_k'(x_{i1}) - \varphi_k'(x_{i2}))$, where x_{i1} and x_{i2} are

x-coordinates of the start and end points of the ith agent, κ is a constant related to material parameters and the gains of the piezoelectric driver and the charge amplifier, and $\varphi_k(x)$ is mode shape function. The dynamic model is a coupled system as the ith actuator's input $u_i(t)$ affects the jth sensor's output $y_j(t)$ through the flexible structure, $i \neq j$, $i, j \in \{1, 2, \ldots, M\}$.

The first three bending modes and four agents are considered in (1), namely, $N = 3$ and $M = 4$. ω_k is calculated directly by the FEM software Abaqus. The calculation of $\psi_{ik}(x)$ has two steps: first, discrete data of $\varphi_k(x)$ is extracted from Abaqus. Second, the analytical expression of $\varphi_k(x)$ is obtained by polynomial fitting, then $\varphi_k'(x)$ is derived through differentiate derivation, and then $\psi_{ik}(x)$ is calculated. κ is calculated and verified by comparison with the physical system. Readers can refer [19] for the calculation method of κ. Parameters are given as

$$\begin{aligned} \boldsymbol{\Omega} &= \text{diag}(0.2745, 2.9446, 9.2524) \times 2\pi \ (\text{rad/s}) \\ \boldsymbol{H} &= 2\boldsymbol{\Omega} \times \text{diag}(0.003, 0.003, 0.003) \\ \boldsymbol{\Psi} &= \begin{bmatrix} 0.0717 & -0.7374 & 1.9776 \\ 0.0699 & -0.5958 & 1.2029 \\ 0.0665 & -0.4444 & 0.4020 \\ 0.0630 & -0.2977 & -0.3216 \end{bmatrix}. \end{aligned} \tag{2}$$

Let $d(t)$ be the voltage signal applied to A_d, and $\boldsymbol{\psi}_d = 2[\psi_{11}, \ldots, \psi_{1N}]^T$.

III. CMPPF Controller Design

A. Multiagent Multimode Controller

MPPF controller of ith agent and kth mode is

$$\begin{cases} \ddot{\mu}_{ik}(t) + \eta_{ck}\dot{\mu}_{ik}(t) + \omega_{ck}^2\mu_{ik}(t) = \omega_{ck}^2 y_i(t) \\ \dot{v}_{ik}(t) + \omega_{ck}v_{ik}(t) = \omega_{ck}y_i(t) \\ u_{ik}(t) = \alpha_{ik}\mu_{ik}(t) + \beta_{ik}v_{ik}(t) \end{cases} \tag{3}$$

where $\alpha_{ik} \in \mathbb{R}$ and $\beta_{ik} \in \mathbb{R}$ are controller gains, $\eta_{ck} = 2\zeta_{ck}\omega_{ck}$ with ζ_{ck} and ω_{ck} being the damping ratio and frequency of controller, respectively. The first equation is the stiffness compensator providing large feedback value of μ_i for enough reduction of force vibration amplitude. The second equation is the damping compensator for high damping ratio. As discussed in [4], the damping ratio and the frequency are chosen as $\zeta_{ck} \ll \zeta_k$ and $\omega ck = \omega_k$, respectively.

Generally, a finite-number modes $N_c \leq N$ are considered. The multimode MPPF for M agents is described as

$$\begin{cases} \ddot{\boldsymbol{\mu}}(t) + \boldsymbol{H}_c\dot{\boldsymbol{\mu}}(t) + \boldsymbol{\Omega}_c^2\boldsymbol{\mu}(t) = \boldsymbol{\Omega}_c^2\boldsymbol{Y}(t) \\ \dot{\boldsymbol{v}}(t) + \boldsymbol{\Omega}_c\boldsymbol{v}(t) = \boldsymbol{\Omega}_c\boldsymbol{Y}(t) \\ \boldsymbol{u}(t) = \boldsymbol{A}\boldsymbol{\mu}(t) + \boldsymbol{B}\boldsymbol{v}(t) \end{cases} \tag{4}$$

where $\boldsymbol{\mu}(t), \boldsymbol{v}(t) \in \mathbb{R}^{MN_c \times 1}$, $\boldsymbol{H}_c = \text{diag}([\boldsymbol{H}_1, \ldots, \boldsymbol{H}_{N_c}])$, $\boldsymbol{\Omega}_c = \text{diag}([\boldsymbol{\Omega}_1, \ldots, \boldsymbol{\Omega}_{N_c}])$, $\boldsymbol{A} = \text{diag}([\boldsymbol{A}_1, \ldots, \boldsymbol{A}_{N_c}])$, and $\boldsymbol{B} = \text{diag}([\boldsymbol{B}_1, \ldots, \boldsymbol{B}_{N_c}])$. $\boldsymbol{H}_k = \eta_{ck}\boldsymbol{I}_M$, $\boldsymbol{\Omega}_k = \omega_{ck}\boldsymbol{I}_M$, $\boldsymbol{A}_k = \text{diag}([\alpha_{1k}, \ldots, \alpha_{Mk}])$, $\boldsymbol{B}_k = \text{diag}([\beta_{1k}, \ldots, \beta_{Mk}])$. $\boldsymbol{Y}(t) = \boldsymbol{1}_{N_c} \otimes \boldsymbol{y}(t)$, $\boldsymbol{y}(t) \in \mathbb{R}^M$, where $\otimes$ represents Kronecker product.

The convergence condition of MPPF is

$$\begin{cases} \alpha_{ik} > 0, \quad \beta_{ik} > 0 \\ \boldsymbol{\Omega}^2 - \tilde{\boldsymbol{\Psi}}^T(\boldsymbol{A} + \boldsymbol{B})\tilde{\boldsymbol{\Psi}} > 0 \end{cases} \tag{5}$$

where $\tilde{\boldsymbol{\Psi}} = \boldsymbol{1}_{N_c} \otimes \boldsymbol{\Psi}$, $i \in 1, 2, \ldots, M$, $k \in 1, 2, \ldots, N_c$. Matrix $* > 0$ means $*$ is positive-definite [4], [5].

B. Consensus Algorithm Design

In multiagent MPPF, individual controllers are unrelated with each other as no information exchange between different agents. Thus, there is disagreement between agents due to different locations and control parameters. If the consensus algorithm is applied to realize information exchange between different agents, individual controllers can work cooperatively to reduce the disagreement, and better performance will be achieved.

For kth mode and ith agent, the consensus algorithm is described as

$$\begin{cases} \ddot{\mu}_{ik} + \eta_k\dot{\mu}_{ik} + \omega_k^2\mu_{ik} = \displaystyle\sum_{j=1}^{M} a_{ij}(\Delta\dot{\mu}_{ijk} + \Delta\mu_{ijk}) \\ \dot{v}_{ik} + \omega_k v_{ik} = \displaystyle\sum_{j=1}^{M} a_{ij}\Delta v_{ijk} \end{cases} \tag{6}$$

where, $\Delta\dot{\mu}_{ijk} = c_{\dot{\mu}}^{jk}\dot{\mu}_{jk} - c_{\dot{\mu}}^{ik}\dot{\mu}_{ik}$, $\Delta\mu_{ijk} = c_{\mu}^{jk}\mu_{jk} - c_{\mu}^{ik}\mu_{ik}$, and $\Delta v_{ijk} = c_v^{jk}v_{jk} - c_v^{ik}v_{ik} \cdot c_{\dot{\mu}}^{ik}$, $c_{\dot{\mu}}^{ik}$ and c_{μ}^{ik} and $c_v^{ik} \in \mathbb{R}$ are the communication gains.

The objective of the consensus algorithm is

$$\begin{cases} \bar{\mu}_{1k}, \underline{a}r\,\mu_{2k}, \ldots, \bar{\mu}_{Mk} \to \bar{\mu}_k \\ \bar{\dot{\mu}}_{1k}, \bar{\dot{\mu}}_{2k}, \ldots, \bar{\dot{\mu}}_{Mk} \to \bar{\dot{\mu}}_k \\ \bar{v}_{1k}, \bar{v}_{2k}, \ldots, \bar{v}_{Mk} \to \bar{v}_k \\ t \to \infty \end{cases} \tag{7}$$

where $\bar{\mu}_{ik} = c_{\mu}^{ik}\mu_{ik}$, $\bar{\dot{\mu}}_{ik} = c_{\dot{\mu}}^{ik}\dot{\mu}_{ik}$, and $\bar{v}_{ik} = c_v^{ik}v_{ik}$ are chosen as the consensus variables.

CMPPF is derived from (3) and (6) and expressed in an integrated form with M agents and first N_c modes

$$\begin{cases} \ddot{\boldsymbol{\mu}} + (\boldsymbol{H}_c - \boldsymbol{L}_{\dot{\mu}})\dot{\boldsymbol{\mu}} + \left(\boldsymbol{\Omega}_c^2 - \boldsymbol{L}_{\mu}\right)\boldsymbol{\mu} = \boldsymbol{\Omega}_c^2\boldsymbol{Y} \\ \dot{\boldsymbol{v}} + (\boldsymbol{\Omega}_c - \boldsymbol{L}_v)\boldsymbol{v} = \boldsymbol{\Omega}_c\boldsymbol{Y} \\ \boldsymbol{u} = \boldsymbol{A}\boldsymbol{\mu} + \boldsymbol{B}\boldsymbol{v} \end{cases} \tag{8}$$

where $\boldsymbol{L}_{\dot{\mu}} = \text{diag}([\boldsymbol{L}_{\dot{\mu}}^{(1)}, \ldots, \boldsymbol{L}_{\dot{\mu}}^{(N_c)}])$, $\boldsymbol{L}_{\mu}^{(k)} = \boldsymbol{L}\boldsymbol{C}_{\mu}^{(k)}$, and $\boldsymbol{C}_{\dot{\mu}}^{(k)} = \text{diag}([c_{\dot{\mu}}^{1k}, \ldots, c_{\dot{\mu}}^{Mk}])$. $\boldsymbol{L}_{\mu}$ and $\boldsymbol{L}_v$ are constructed in the same way as $\boldsymbol{L}_{\dot{\mu}}$.

As the topology is determined by the physical connections, it should meet a certain condition before the controller design. The condition is given in [20] and reviewed as following. The algorithm expressed by (6) can reach consensus if and only if the topology described by $\boldsymbol{L}$ contains a directed spanning tree. In other words, a subset of the edges exists such that one agent is the parent of the rest of the agents. Thus, $\boldsymbol{L}$ should satisfy that only one eigenvalue is zero and all the others are positive.

C. Convergence Condition

Derived from (1) and (8), the closed-loop system is described as

$$\begin{bmatrix}\ddot{\boldsymbol{q}}\\ \ddot{\boldsymbol{\theta}}\\ \boldsymbol{0}\end{bmatrix}+\tilde{\boldsymbol{H}}\begin{bmatrix}\dot{\boldsymbol{q}}\\ \dot{\boldsymbol{\theta}}\\ \dot{\boldsymbol{\sigma}}\end{bmatrix}+\tilde{\boldsymbol{\Omega}}\begin{bmatrix}\boldsymbol{q}\\ \boldsymbol{\theta}\\ \boldsymbol{\sigma}\end{bmatrix}=\begin{bmatrix}\boldsymbol{\psi}_d d\\ \boldsymbol{0}\\ \boldsymbol{0}\end{bmatrix} \tag{9}$$

where

$$\tilde{\boldsymbol{H}}=\begin{bmatrix}\boldsymbol{H} & \boldsymbol{0} & \boldsymbol{0}\\ \boldsymbol{0} & \boldsymbol{H}_c-\boldsymbol{L}_{\dot{\mu}} & \boldsymbol{0}\\ \boldsymbol{0} & \boldsymbol{0} & \boldsymbol{I}_{m\times N_c}\end{bmatrix}$$

$$\tilde{\boldsymbol{\Omega}}=\begin{bmatrix}\boldsymbol{\Omega}^2 & -\tilde{\boldsymbol{\Psi}}^T\boldsymbol{A} & -\tilde{\boldsymbol{\Psi}}^T\boldsymbol{B}\\ -\boldsymbol{\Omega}_c^2\tilde{\boldsymbol{\Psi}} & \boldsymbol{\Omega}_c^2-\boldsymbol{L}_{\mu} & \boldsymbol{0}\\ -\boldsymbol{\Omega}_c\tilde{\boldsymbol{\Psi}} & \boldsymbol{0} & \boldsymbol{\Omega}_c-\boldsymbol{L}_{\nu}\end{bmatrix}.$$

Theorem 1: For $\lambda_{\mu}^{(k)}$, $\lambda_{\dot{\mu}}^{(k)}$, and $\lambda_{\nu}^{(k)}$ are the maximal eigenvalue of matrix $\boldsymbol{L}_{\mu}^{(k)}$, $\boldsymbol{L}_{\dot{\mu}}^{(k)}$, and $\boldsymbol{L}_{\nu}^{(k)}$, respectively, the closed-loop system described by (9) is asymptotically stable if and only if

$$\begin{cases}\alpha_{ik}>0, \quad \beta_{ik}>0\\ \lambda_{\dot{\mu}}^{(k)}<\eta_k, \quad \lambda_{\mu}^{(k)}<{\omega_k}^2, \quad \lambda_{\nu}^{(k)}<\omega_k\\ \boldsymbol{\Omega}^2-\tilde{\boldsymbol{\Psi}}^T(\tilde{\boldsymbol{A}}+\tilde{\boldsymbol{B}})\tilde{\boldsymbol{\Psi}}>0\end{cases} \tag{10}$$

where

$$\begin{cases}\tilde{\boldsymbol{A}}=\boldsymbol{A}\left(\boldsymbol{I}_{M\times N_c}-\boldsymbol{L}_{\mu}\boldsymbol{\Omega}_c^{-2}\right)^{-1}\\ \tilde{\boldsymbol{B}}=\boldsymbol{B}\left(\boldsymbol{I}_{M\times N_c}-\boldsymbol{L}_{\nu}\boldsymbol{\Omega}_c^{-1}\right)^{-1}\\ k\in 1,2,\ldots,N_c.\end{cases} \tag{11}$$

Proof: The closed-loop system described by (9) is asymptotically stable if and only if [19]

$$\tilde{\boldsymbol{H}}>0, \quad \tilde{\boldsymbol{\Omega}}>0. \tag{12}$$

Necessary conditions to (12) are $\boldsymbol{H}_c-\boldsymbol{L}_{\dot{\mu}}>0$, and $\boldsymbol{\Omega}_c-\boldsymbol{L}_{\nu}>0$ & $\boldsymbol{\Omega}_c^2-\boldsymbol{L}_{\mu}>0$. Then $\lambda_{\dot{\mu}}^{(k)}<\eta_k$, $\lambda_{\mu}^{(k)}<{\omega_k}^2$ and $\lambda_{\nu}^{(k)}<\omega_k$.

If $\boldsymbol{D}$ is inversible, the Schur complement of the block $\boldsymbol{D}$ of the matrix $\boldsymbol{M}=\begin{bmatrix}\boldsymbol{A} & \boldsymbol{B}\\ \boldsymbol{C} & \boldsymbol{D}\end{bmatrix}$ is

$$\boldsymbol{M}/\boldsymbol{D}:=\boldsymbol{A}-\boldsymbol{B}\boldsymbol{D}^{-1}\boldsymbol{C}.$$

$\boldsymbol{M}>0$ is equivalent to $\boldsymbol{D}>0$ and $\boldsymbol{M}/\boldsymbol{D}>0$. The equivalent condition of $\tilde{\boldsymbol{\Omega}}>0$ can be derived using Schur complement

$$\boldsymbol{\Omega}^2-\tilde{\boldsymbol{\Psi}}^T(\tilde{\boldsymbol{A}}+\tilde{\boldsymbol{B}})\tilde{\boldsymbol{\Psi}}>0.$$

Theorem 1 is proved.

D. Consensus Parameters Optimization

In real applications, the internal control parameters $\boldsymbol{A}_k$ and $\boldsymbol{B}_k$ need to be adjusted for each agent. To reduce the complexity, the differences between internal control parameters are not taken into consideration. Thus, all agents share the same set of internal control parameters, namely, $\boldsymbol{A}_k=\alpha_k\boldsymbol{I}$ and $\boldsymbol{B}_k=\beta_k\boldsymbol{I}$ with $\boldsymbol{I}\in\mathbb{R}^{M\times M}$. However, as they play different roles in the network, communication gains $\boldsymbol{C}_{\mu}$, $\boldsymbol{C}_{\dot{\mu}}$, and $\boldsymbol{C}_{\nu}$ for different agents that are treated to be different. The system is easy to expand such as change of the number of agents, as communication gains are the only parameters need to be adjusted during expanding, rather than the internal control parameters.

AFR is used to evaluate the control performance. If $G_c(s)$ is a closed-loop transfer function, AFR amplitude with the unit "dB" is $\|G_c(s)\|=20\log(|G_c(j\omega)|)$, where j is the imaginary unit, $\omega\in[0,\infty)$. Lower AFR amplitude means lower amplitude of vibration with the same disturbance.

Derived from (1) and (8), the closed-loop system from the disturbance to ith sensor is rewritten as

$$\begin{cases}\dot{\boldsymbol{x}}=\boldsymbol{A}_{\text{cons}}\boldsymbol{x}+\boldsymbol{B}_{\text{cons}}d\\ y_i=\boldsymbol{C}_{\text{cons}}^i\boldsymbol{x}\end{cases} \tag{13}$$

where $\boldsymbol{A}_{\text{cons}}$ contains α_k, β_k, $\boldsymbol{C}_{\dot{\mu}}^{(k)}$, $\boldsymbol{C}_{\mu}^{(k)}$, and $\boldsymbol{C}_{\nu}^{(k)}$

$$\boldsymbol{x}=[q_1,\dot{q}_1,\ldots,q_N,\dot{q}_N,\mu_1,\dot{\mu}_1,\nu_1,\ldots,\mu_M,\dot{\mu}_M,\nu_M]^T$$
$$\boldsymbol{B}_{\text{cons}}=[0,\psi_{d1},\ldots,0,\psi_{dN},\boldsymbol{0}^{3MN_c}]^T$$
$$\boldsymbol{C}_{\text{cons}}^i=[\psi_{i1},0,\ldots,\psi_{iN},0,\boldsymbol{0}^{3MN_c}].$$

The closed-loop system described by (13) is expected to have not only the smallest supremum of response amplitudes but also the smallest response amplitude at the control frequency. These criterions are described as H_{∞} norm and the AFR amplitude at the control frequency, respectively.

Closed-loop transfer function from d to y_i is

$$G_i(s)=\boldsymbol{C}_{\text{cons}}^i[s\boldsymbol{I}_{2N+3MN_c}-\boldsymbol{A}_{\text{cons}}]^{-1}\boldsymbol{B}_{\text{cons}}. \tag{14}$$

H_{∞} norm is described as

$$\|G_i(s)\|_{\infty}=20\log(\sup_{\omega}\sigma_{\max}(G_i(j\omega))) \tag{15}$$

where $\sigma_{\max}$ is the maximum eigenvalue.

The AFR amplitude at control frequency ω_k is described as

$$\|G_i(s)\|_{\omega_k}=20\log(|G_i(j\omega_k)|). \tag{16}$$

First of all, the controller gains α_k and β_k are chosen based on (15) and (16). $G_i(s)$ is transformed to the closed-loop transfer function of multiagent MPPF if $\boldsymbol{C}_{\mu}=\boldsymbol{0}$, $\boldsymbol{C}_{\dot{\mu}}=\boldsymbol{0}$, and $\boldsymbol{C}_{\nu}=\boldsymbol{0}$. Proper values of α_k and β_k are calculated to meet $\|G_i(s)\|_{\omega_k}<G_{\omega_k}^*$ and $\|G_i(s)\|_{\infty}<G_H^*$. $G_{\omega_k}^*$ and G_H^* are the target values corresponding to the desired control performance. Then let $\boldsymbol{C}_{\mu}\neq\boldsymbol{0}$, $\boldsymbol{C}_{\dot{\mu}}\neq\boldsymbol{0}$, and $\boldsymbol{C}_{\nu}\neq\boldsymbol{0}$, $G_i(s)$ describes the ith closed-loop transfer function in CMPPF.

The optimal target function is defined as

$$J_{\text{cons}}=\sum_{i=1}^{m}\left(\gamma_{\infty}\|G_i(s)\|_{\infty}+\sum_{k=1}^{N_c}\gamma_{\omega_k}\|G_i(s)\|_{\omega_k}\right). \tag{17}$$

The $||G_i(s)||_{\infty}$ represents the maximum AFR. While the $||G_i(s)||_{\omega_k}$ provides AFR at control frequencies. Thus, parameters γ_{∞} and γ_{ω} in (17) provide a balance between $||G_i(s)||_{\infty}$ and $||G_i(s)||_{\omega_k}$. The higher γ_{∞} is, a smaller $||G_i(s)||_{\infty}$ will be obtained. During the minimization of J_{cons}, different results of consensus parameters $\boldsymbol{C}_{\dot{\mu}}^{(k)}$, $\boldsymbol{C}_{\mu}^{(k)}$, and $\boldsymbol{C}_{\nu}^{(k)}$ will be obtained and different control performances are realized with different γ_{∞} and γ_{ω}. Several iterative adjustments of γ_{∞} and γ_{ω} are usually needed based on experience and the design requirement.

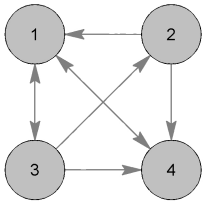

Fig. 4. Communication topology of the CMPPF agents.

IV. Simulations and Results

A. Controller Design

Three bending modes are considered in the dynamic model in Section II, namely, $N = 3$. In order to determine the control modes, a maneuver experiment is performed and the vibration of the flexible structure is measured. Through the fast Fourier transformation (FFT) analysis of measured data from the sensor S_1, first two modal vibrations are excited with corresponding FFT peaks, and the third and above modal vibrations are not excited with no corresponding peaks. Based on this, the first two modes are mainly considered in controller design, namely, $N_c = 2$.

Based on the discussion about $\boldsymbol{L}$ in Section III-B, a communication topology with a directed spanning tree is shown in Fig. 4. The corresponding Laplacian matrix is

$$\boldsymbol{L} = \begin{bmatrix} 3 & -1 & -1 & -1 \\ 0 & 1 & -1 & 0 \\ -1 & 0 & 1 & 0 \\ -1 & -1 & -1 & 3 \end{bmatrix}. \tag{18}$$

Based on (5) and [4], a maximum value of $(\alpha_1+\beta_1+\alpha_2+\beta_2)$ is calculated

$$M_{\max} = \sigma_{\max}(\boldsymbol{\Omega}^2(\boldsymbol{\Psi}\boldsymbol{\Psi}^T)^{-1}). \tag{19}$$

The values of $G^*_{\omega_k}$ and G^*_H are chosen as -70 and -30 dB, respectively. Small value of α_k and large value of β_k are chosen to satisfy $\|G_i(s)\|_{\omega_k} < G^*_{\omega_k}$ and $\|G_i(s)\|_\infty < G^*_H$

$$\begin{cases} \alpha_1 = \alpha_2 = 0.3M_{\max} = 1.4020 \\ \beta_1 = \beta_2 = 4M_{\max} = 37.3872. \end{cases} \tag{20}$$

Let $\gamma_\infty = \gamma_\omega = 1$, consensus parameters in CMPPF are calculated

$$\begin{cases} \boldsymbol{C}^{(1)}_{\dot{\mu}} = \text{diag}(0.0007, -0.0262, -0.0788, -0.0987) \\ \boldsymbol{C}^{(2)}_{\dot{\mu}} = \text{diag}(0.0040, -0.1000, -0.0857, -0.0901) \\ \boldsymbol{C}^{(1)}_{\mu} = \text{diag}(0.0025, 0.0848, -0.0704, -0.0627) \\ \boldsymbol{C}^{(2)}_{\mu} = \text{diag}(0.0968, 0.0986, -0.0622, -0.0021) \\ \boldsymbol{C}^{(1)}_{v} = \text{diag}(-0.0995, 0.0246, -0.0996, 0.1000) \\ \boldsymbol{C}^{(2)}_{v} = \text{diag}(0.0691, 0.0794, 0.1000, 0.0931). \end{cases} \tag{21}$$

AFR from A_d to S_1 is analyzed to compare MPPF and CMPPF. $\alpha_{1,2}$ and $\beta_{1,2}$ in (20) are used in MPPF, while parameters in (20) and (21) are used in CMPPF. AFR amplitudes of closed-loop transfer functions of MPPF and CMPPF are shown in Fig. 5. "NC" means noncontrolled system in the legend. The AFR amplitudes of CMPPF and MPPF are much lower than that of noncontrolled system at the resonant frequencies. The AFR amplitude of CMPPF is -98.46 dB, lower than -70.34 dB of MPPF at 0.2745 Hz. The AFR amplitude of CMPPF is -103.30 dB, much lower than -78.48 dB of MPPF at 2.9446 Hz. More than 20 dB is further reduced by CMPPF at both resonant frequencies. Fig. 6 shows the subfigures in Fig. 5. There are two unexpected peaks in the curves of MPPF at $p_1(0.2739, -45.39)$ and $p_2(2.941, -55.32)$, due to the disagreement between different agents in multimode MPPF. The two peaks do not exist in single-agent MPPF designed in [21]. However, the two peaks do not exist in the curve of CMPPF in Fig. 6. Results indicate that CMPPF successfully eliminates the disagreement between agents.

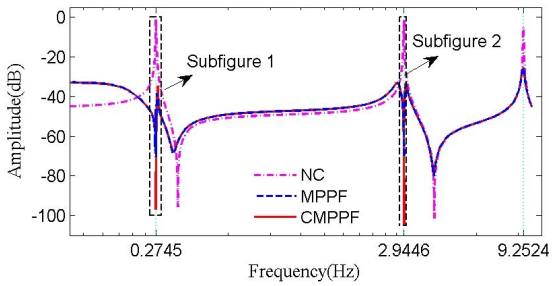

Fig. 5. AFR of closed-loop system of CMPPF and MPPF.

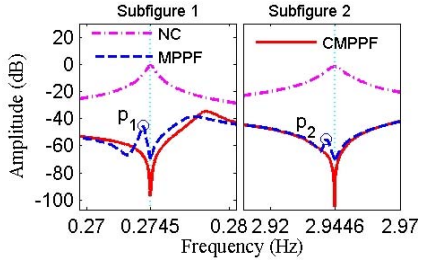

Fig. 6. Subfigures in Fig. 5.

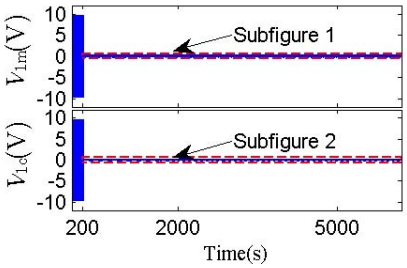

Fig. 7. Measured voltage of S_1 controlled by MPPF and CMPPF.

B. Simulation Result Without Agents Failure

Numerical simulations are carried out by applying periodic disturbance d_d to A_d

$$d_d = 10\sin(\omega_1 t) + \sin(\omega_2 t) \tag{22}$$

where $\omega_1 = 0.2745$ Hz and $\omega_2 = 2.9446$ Hz. In the following figures and variables, subscribes (m) and (c) represent MPPF and CMPPF, respectively.

The root torque is a key indicator for the vibration of the flexible structure in spacecraft. Let $V_1 = y_1$, V_1 is proportional to the root torque of the flexible structure. It is used to evaluate the controller performance in Figs. 7 and 8. In Fig. 7,

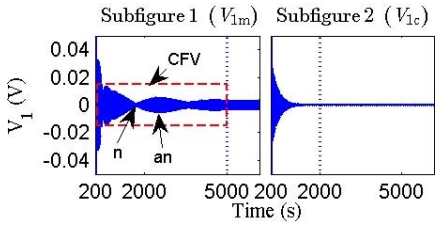

Fig. 8. Subfigures in Fig. 7.

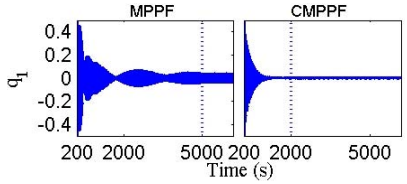

Fig. 9. Generalized modal coordinate q_1 in MPPF and CMPPF.

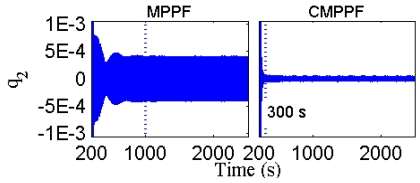

Fig. 10. Generalized modal coordinate q_2 in MPPF and CMPPF.

V_{1m} and V_{1c} are the amplitude of V_1 of MPPF and CMPPF, respectively. They have the amplitudes of 9.045 V before 200 s due to the force vibration of the flexible structure. After control is added at 200 s, the amplitudes are rapidly attenuated by CMPPF (V_{1c}) and MPPF (V_{1m}). Fig. 8 shows the details after 200 s. The amplitude and the time reaching steady state are defined as a steady-state amplitude (SSA) and steady-state time. SSA of V_{1c} is 1.05×10^{-4} V after 2000 s, while that of V_{1m} is 3.26×10^{-3} V after 5000 s. Clap-frequency vibration (CFV) is found in V_{1m} before 5000 s. CFV is obvious when the difference between two frequencies is less than 20% of the average frequency as described in [22]. Its curve has nodes (n) and antinodes (an) as shown in Fig. 8. CFV leads to the slow attenuation process of MPPF. It reflects the effect of the unexpected peaks, whose frequencies are near to the disturbance frequencies.

Generalized modal coordinates $q_{1,2}$ are given in Figs. 9 and 10. q_1 in MPPF shows the CFV at first modal frequency before 5000 s. q_1 in MPPF reaches SSA 0.0436 after 5000 s, while q_1 in CMPPF reaches SSA 0.001 after 2000 s. The amplitude of q_2 is much lower than that of q_1. There is also a CFV before 1000 s in MPPF. q_2 in MPPF reaches SSA 4.0×10^{-4} after 1000 s, while q_2 in CMPPF reaches SSA 6.0×10^{-5} after 300 s. Both q_1 and q_2 are faster and more attenuated by CMPPF.

The disagreements of consensus variables are quantified by their standard deviations of four agents. $s_\mu^{(k)}$, $s_{d\mu}^{(k)}$, and $s_\nu^{(k)}$ are the standard deviations of $\{\bar{\mu}_{1k}, \ldots, \bar{\mu}_{4k}\}$, $\{\dot{\bar{\mu}}_{1k}, \ldots, \dot{\bar{\mu}}_{4k}\}$, and $\{\bar{\nu}_{1k}, \ldots, \bar{\nu}_{4k}\}$ for the kth mode, respectively. Figs. 11 and 12 show the upper envelopes of $s_\mu^{(1,2)}$, $s_{d\mu}^{(1,2)}$, and $s_\nu^{(1,2)}$, respectively.

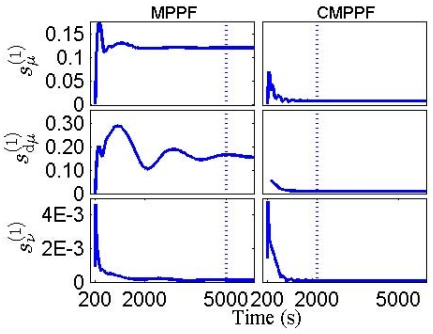

Fig. 11. Consistency analysis of first modal control of MPPF and CMPPF.

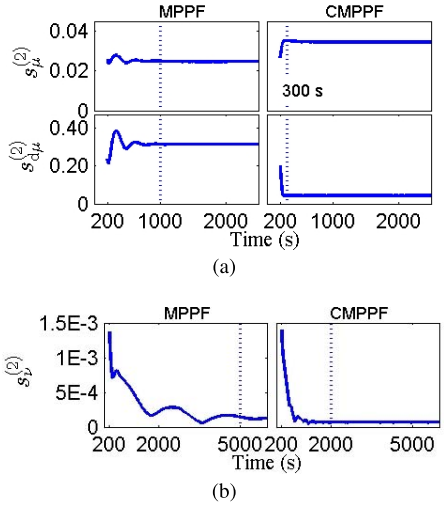

Fig. 12. Consistency analysis of second modal control of MPPF and CMPPF. (a) $s_\mu^{(2)}$ and $s_{d\mu}^{(2)}$. (b) $s_\nu^{(2)}$.

For the first mode, $s_\mu^{(1)}$, $s_{d\mu}^{(1)}$, and $s_\nu^{(1)}$ reach steady-state values after 2000 s in CMPPF, while it takes 5000 s in MPPF. Quicker convergence processes and lower steady-state values are achieved by CMPPF than MPPF. For MPPF, there are some fluctuations in the curves before 5000 s, especially in $s_{d\mu}^{(1)}$. These fluctuations are not found in CMPPF.

For the second mode, both $s_\mu^{(2)}$ and $s_{d\mu}^{(2)}$ reach steady-state values after 300 s in CMPPF, while it takes 1000 s in MPPF. The steady-state value of $s_{d\mu}^{(2)}$ of CMPPF is lower than that of MPPF. However, the steady-state value of $s_\mu^{(2)}$ of CMPPF is a little higher than that of MPPF. Even so, lower amplitude of q_2 is achieved by CMPPF than MPPF (Fig. 10). Based on this, we can infer that the convergence of $s_{d\mu}^{(2)}$ has stronger effect on controller performance than that of $s_\mu^{(2)}$.

$s_\nu^{(2)}$ of MPPF reaches steady-state value after 5000 s, while that of CMPPF reaches slightly lower steady-state value after 2000 s. This result indicates that $s_\nu^{(2)}$ is affected by the first modal vibration control. However, $s_\nu^{(1,2)}$ is much lower than $s_{d\mu}^{(1,2)}$ and $s_\mu^{(1,2)}$ both in MPPF and CMPPF. It means that there is consistency in $\bar{\nu}_{ik}$ even without the consensus algorithm.

Judging from all evidence offered, we may reasonably deduce the conclusion that the better performance of CMPPF comes from the consensus of the chosen consensus variables. In the simulation example, the order of importance of consensus variables is $\dot{\bar{\mu}}_{ik} > \bar{\mu}_{ik} \gg \bar{\nu}_{ik}$, sorted by the effect on vibration control.

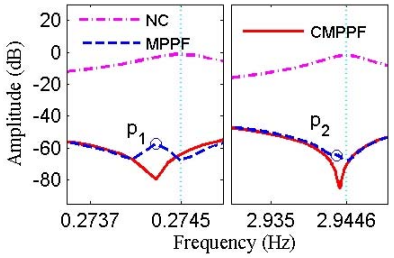

Fig. 13. AFR near resonant frequencies with agents #1 and #3 failure.

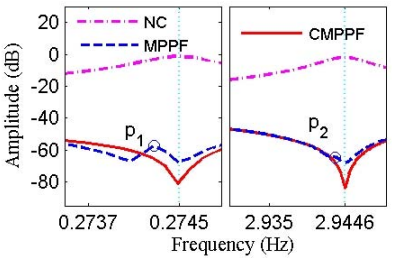

Fig. 14. AFR near resonant frequencies with agents #1 and #3 failure and $\boldsymbol{C}_{\mu}^{(1,2)}$ set to zeros.

C. Simulation Result With Agents Failure

Further simulations are carried out with one or two agents failure. The ith agent failure means the computer in the ith agent is not able to calculate the controller signal, that is $\mu_i = 0$, $v_i = 0$ and $u_i = 0$. AFR amplitudes at resonant frequencies are chosen as control performance indicators. A typical case with agents #2 and #4 failure is chosen to illustrate the failure status. AFR near the resonant frequencies is shown in Fig. 13. The unexpected peaks $p_1(0.2742, -57.42)$ and $p_2(2.943, -64.47)$ are lower than that without agents failure (Fig. 6), especially p_2 is not obvious. This indicates that less disagreement is generated with only two agents left. AFR gains of MPPF at resonant frequencies are -67.73 and -68.18 dB, respectively. They are a little higher than that without agents failure because of the failure of two agents. For CMPPF, however, the lowest points are $(0.2742, -79.83)$ and $(2.944, -85.21)$. They are not exactly at the resonant frequencies. There are frequency shifts of 0.0003 and 0.0006 Hz at the first and second mode, respectively. Due to the frequency shifts, the lowest AFR amplitudes are not at the resonant frequencies. This phenomenon is unwanted. However, if we set $\boldsymbol{C}_{\mu}^{(1,2)}$ to zeros, the frequencies shifts are reduced to very small values, as shown in Fig. 14. This approach does not affect the controller performance without agents failure. Thus, it can be seen that in some cases, the consensus of $\bar{\mu}_{ik}$ brings negative effect on CMPPF vibration control. This is a proof to the order of importance of consensus variables $\bar{\mu}_{ik} > \bar{\mu}_{ik}$.

Results of 10 failure types are listed in Table II. The first column stands for failure types, where "0" and "1" represent failure and normal for the four agents, respectively. For example, "1010" means agent #2 and #4 are in failure mode, while agent #1 and #3 are normal. "FS" means frequency shift with the unit "Hz." For most types, CMPPF achieves lower AFR gains than MPPF with some frequencies shifts. These frequencies shifts are all reduced to very small after setting $\boldsymbol{C}_{\mu}^{(1,2)}$ to zeros. However, for failure modes "0111," "0011," "0101," and "0110," CMPPF performs not better than MPPF. The similarity of these four types is that agent #1 is in failure mode. This phenomenon indicates that different agents have different importance in CMPPF. The related investigation will be considered in future studies.

TABLE II
RESULTS OF 10 FAILURE TYPES

	1st resonant frequency			2nd resonant frequency		
	MPPF	CMPPF		MPPF	CMPPF	
	AFR	AFR	FS	AFR	AFR	FS
0111	-59.87	-52.90	0.0046	-60.31	-53.27	0.0048
1011	-67.91	-83.74	0.0001	-68.11	-88.48	0.0006
1101	-70.25	-77.90	0.0003	-70.46	-111.82	0.0011
1110	-69.38	-97.00	0.0001	-70.11	-87.79	0.0004
0011	-49.93	-45.59	0.0017	-48.44	-43.27	0.0033
1001	-67.43	-71.69	0.0003	-67.56	-100.30	0.0011
1100	-71.07	-72.27	0.0003	-71.30	-92.63	0.0013
0101	-59.55	-46.15	0.0046	-59.95	-46.70	0.0021
1010	-67.73	-79.83	0.0002	-68.18	-85.21	0.0008
0110	-58.76	-48.62	0.0046	-60.26	-51.69	0.0027

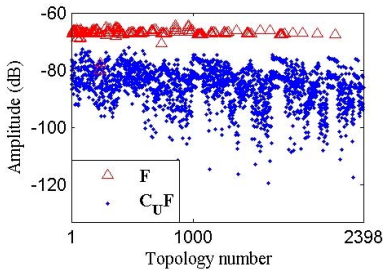

Fig. 15. AFR amplitudes at first resonant frequency for 2398 topologies.

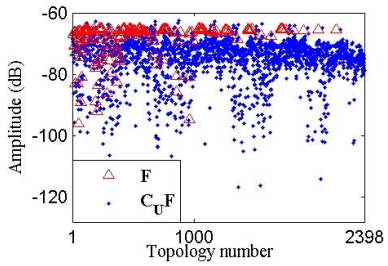

Fig. 16. AFR amplitudes at second resonant frequency for 2398 topologies.

D. Controller Robustness to Different Topologies

There are 4096 possible topologies for the system with four agents. Among them, a subset $\mathbf{U}$ includes 2398 topologies such that a topology has a directly spanning tree, which satisfies the choice principle in Section II-B. AFR amplitudes $\|G_1(s)\|_{\omega_1}$ and $\|G_1(s)\|_{\omega_2}$ with topology $g \in \mathbf{U}$ are given in Figs. 15 and 16. $\mathbf{F}$ is defined as a subset of $\mathbf{U}$ including the topologies with no edges rooting at agent 1. $\mathbf{F}$ has 189 elements. $\mathbf{C_U F}$ is the complementary set of $\mathbf{F}$ in $\mathbf{U}$. $\|G_1(s)\|_{\omega_1}$ is near the AFR amplitude -70.34 dB of MPPF with $g \in \mathbf{F}$ and much lower than -70.34 dB with $g \in \mathbf{C_U F}$. The conclusion is not obvious but still generally satisfied at the second frequency. It reveals that the control performance

is improved by the consensus algorithm if the information of agent #1 is introduced into other agents. The reason is the important role of agent #1 with $|\psi_{11}|$ and $|\psi_{12}|$ the largest among $|\psi_{11}|$ to $|\psi_{41}|$ and $|\psi_{12}|$ to $|\psi_{42}|$, respectively. Communication topology $g \in \mathbf{C_U F}$ could be an additional choice principle for communication topologies. However, the controller performance is not worse with $g \in \mathbf{U}$. It indicates that the controller is robust with different communication topologies. The probability is 92.12% (2209 out of 2398) for controller performance improvement by the consensus algorithm with different topologies.

V. Conclusion

An AVC method CMPPF is introduced based on the consensus algorithm and centralized MPPF. The convergence conditions are derived and control parameters are optimized. Control performances of CMPPF and MPPF are analyzed and compared via AFR and numerical simulations. Agents' disagreement is eliminated and lower AFR amplitudes are achieved by CMPPF. Better attenuation process and lower steady-state value are achieved by CMPPF than MPPF. How CMPPF achieving better performance is illustrated through analysis on consensus variables. Different effects of consensus variables are analyzed. Control performances under different failure types are evaluated. Results show that CMPPF achieves lower AFR gains at resonant frequencies than MPPF for most failure types. Results also reveal that different agents have different importance in CMPPF. Furthermore, the robustness of CMPPF to different topologies is demonstrated by employing all possible communication topologies with a directed spanning tree. Investigations about the different effects of consensus variables and the different importance of agents will be considered in future studies.

Acknowledgment

The authors would like to thank Prof. A. Serrani, Editor-in-Chief, Dr. Y. Ebihara, Associate Editor, and the anonymous reviewers for their constructive comments, which helped improve the quality and presentation of this brief.

References

[1] B. Wie and C. M. Roithmayr, "Attitude and orbit control of a very large geostationary solar power satellite," *J. Guid., Control, Dyn.*, vol. 28, no. 3, pp. 439–451, 2005.

[2] B. Wie and M. Gonzalez, "Control synthesis for flexible space structures excited by persistent disturbances," *J. Guid., Control, Dyn.*, vol. 15, no. 1, pp. 73–80, 1992.

[3] S. O. R. Moheimani, B. J. G. Vautier, and B. Bhikkaji, "Experimental implementation of extended multivariable PPF control on an active structure," *IEEE Trans. Control Syst. Technol.*, vol. 14, no. 3, pp. 443–455, May 2006.

[4] S. N. Mahmoodi and M. Ahmadian, "Active vibration control with modified positive position feedback," *J. Dyn. Syst., Meas. Control*, vol. 131, no. 4, pp. 041002-1–041002-8, 2009.

[5] E. Omidi and S. N. Mahmoodi, "Novel hybrid positive feedback control for active vibration suppression in flexible structure," in *Proc. Amer. Control Conf.*, Portland, OR, USA, Jun. 2014, pp. 2723–2728.

[6] S. N. Mahmoodi and M. Ahmadian, "Active control of structures with adaptive modified positive position feedback," *Proc. SPIE*, vol. 7977, pp. 79770E-1–79770E-20, Apr. 2011.

[7] H. Nobahari, S. A. H. Kordkheili, and S. S. Afshari, "Hardware-in-the-loop optimization of an active vibration controller in a flexible beam structure using evolutionary algorithms," *J. Intell. Mater. Syst. Struct.*, vol. 25, no. 10, pp. 1211–1223, 2014.

[8] E. Omidi and S. N. Mahmoodi, "Implementation of H_∞ modified positive position and velocity feedback controllers for active vibration control of flexible structures in multimode," in *Proc. Amer. Control Conf.*, Portland, OR, USA, Jun. 2014, pp. 2735–2740.

[9] Z. Wang and T. Li, "Optimal Piezoelectric sensor/actuator placement of cable net structures using H_2 norm measures," *J. Vibrat. Control*, vol. 20, no. 8, pp. 1257–1268, 2014.

[10] M. S. Saad, H. Jamaluddin, and I. Z. M. Darus, "Online monitoring and self-tuning control using pole placement method for active vibration control of exible beam system," *J. Vibrat. Control*, vol. 21, no. 3, pp. 449–460, 2013.

[11] E. Omidi and S. N. Mahmoodi, "Consensus positive position feedback control for vibration attenuation of smart structures," *Smart Mater. Struct.*, vol. 24, pp. 045016-1–045016-11, 2015.

[12] E. Omidi and S. N. Mahmoodi, "Vibration suppression of distributed parameter flexible structures by integral consensus control," *J. Sound Vibrat.*, vol. 364, pp. 1–13, Mar. 2016.

[13] E. Omidi and S. N. Mahmoodi, "Active vibration control of structures using a leader–follower-based consensus design," *J. Vibrat. Control*, vol. 24, no. 1, pp. 60–72, 2016, doi: 10.1177/.1077546316631896.

[14] J. R. T. Lawton, R. W. Beard, and B. J. Young, "A decentralized approach to formation maneuvers," *IEEE Trans. Robot. Autom.*, vol. 19, no. 6, pp. 933–941, Dec. 2003.

[15] W. Ren and R. W. Beard, "Decentralized scheme for spacecraft formation flying via the virtual structure approach," *J. Guid., Control Navigat.*, vol. 27, no. 1, pp. 73–82, 2004.

[16] J. A. Fax and R. M. Murray, "Information flow and cooperative control of vehicle formations," *IEEE Trans. Autom. Control*, vol. 49, no. 9, pp. 1465–1476, Sep. 2004.

[17] W. Ren and R. W. Beard, "Consensus seeking in multiagent systems under dynamically changing interaction topologies," *IEEE Trans. Autom. Control*, vol. 50, no. 5, pp. 655–661, May 2005.

[18] M. R. Anderson and A. C. Robbins, "Formation flight as a cooperative game," in *Proc. AIAA Guid. Navigat. Control Conf.*, Boston, MA, USA, 1998, p. 244.

[19] S. O. R. Moheimani and J. F. Andrew, *Piezoelectric Transducers for Vibration Control and Damping*. Berlin, Germany: Springer, 2006.

[20] W. Ren, "On consensus algorithms for double-integrator dynamics," *IEEE Trans. Autom. Control*, vol. 53, no. 6, pp. 1503–1509, Jul. 2008.

[21] E. Omidi and S. N. Mahmoodi, "Active Vibration control of resonant systems via multivariable modified positive position feedback," in *Proc. ASME Dyn. Syst. Control Conf.*, 2013, p. V003T48A001.

[22] R. T. Buscarello, *Practical Solutions to Machinery and Maintenance Vibration Problems*, 4th ed. Denver, CO, USA: Update International, 2002.